Title: Genome size evolution and phenotypic correlates in the poison frog family Dendrobatidae

Running Title: Evolutionary changes in poison frog genome size

Authors: Tyler E. Douglas[1,*,†], Roberto Márquez[2,*,†], V. Renee Holmes[3], J. Spencer Johnston[3], and Rebecca D. Tarvin[1,†]

*contributed equally

† corresponding author

[1] Museum of Vertebrate Zoology and Department of Integrative Biology, University of California, Berkeley, CA 94720 USA

[2] Department of Ecology and Evolutionary Biology and Michigan Society of Fellows, University of Michigan, Ann Arbor, MI. 48109. USA

[3] Department of Entomology, Texas A&M University, College Station, TX 77843 USA

Author emails: tyler.douglas@berkeley.edu, marquezr@umich.edu, vrh0933406@tamu.edu, J.Johnston@ag.tamu.edu, rdtarvin@berkeley.edu

Abstract

Adaptive and neutral processes have produced a spectrum of genome sizes across organisms. Amphibians in particular possess a wide range in C-values, from <1 pg to over 125 pg. However, the genome size of most amphibians is unknown, and no single family has been comprehensively assessed. We provide new estimates for 32 poison frog species representing the major lineages within Dendrobatidae using Feulgen staining of museum specimens and flow cytometry of fresh tissue. We show that genome size in Dendrobatidae likely evolves under an Ornstein–Uhlenbeck process, potentially with evolutionary rate shifts in the genera *Phyllobates* and *Hyloxalus*, which respectively possess species with the largest (13.0 pg) and second smallest (2.6 pg) genomes in the family. Phylogenetically controlled analyses indicate that genome size is positively correlated with snout-vent-length, oocyte number, and clutch size, but negatively correlated with active metabolic rate and metabolic scope. While body size and metabolic rate are also correlates of toxicity, we found no relationship between genome size and the evolution of chemical defense within Dendrobatidae. Our assessment of genome size in Dendrobatidae provides insight into the processes shaping genome size evolution over short timescales and a dataset that will facilitate investigations of the mechanistic links between genome size and organismal physiology.

Keywords: transposable elements, metabolic rate, amphibians, phenotypic evolution

Resumen

Los procesos adaptativos y neutrales han producido un espectro de tamaños de genoma en los organismos. Los anfibios en particular poseen una amplia gama de valores C, desde <1 pg hasta más de 125 pg. Sin embargo, se desconoce el tamaño del genoma de la mayoría de los anfibios y no se ha evaluado exhaustivamente ninguna familia. Proporcionamos nuevas estimaciones para

32 especies de ranas venenosas que representan los principales linajes dentro de Dendrobatidae utilizando la tinción de Feulgen con especímenes de museo y citometría de flujo con tejido fresco. Mostramos que el tamaño del genoma en Dendrobatidae probablemente evolucione bajo un proceso de Ornstein-Uhlenbeck, potencialmente con cambios en la tasa evolutiva en los géneros *Phyllobates* e *Hyloxalus*, que respectivamente poseen especies con el genoma más grande (13,0 pg) y el segundo más pequeño (2,6 pg) de la familia. Los análisis filogenéticamente controlados indican que el tamaño del genoma se correlaciona positivamente con la longitud hocico-cloaca, el número de ovocitos y el tamaño de la nidada, pero se correlaciona negativamente con la tasa metabólica activa y el alcance metabólico. Aunque el tamaño corporal y la tasa metabólica se correlacionan con la toxicidad, no encontramos relación entre el tamaño del genoma y la evolución de la defensa química dentro de Dendrobatidae. Nuestra evaluación del tamaño del genoma en Dendrobatidae proporciona información sobre los procesos que dirigen la evolución del tamaño del genoma en escalas de tiempo cortas y un conjunto de datos que facilitará las investigaciones de los vínculos mecánicos entre el tamaño del genoma y la fisiología del organismo.

Palabras clave: Elementos transponibles, tasa metabólica, anfibios, evolución fenotípica

DataDryad DOI: 10.5061/dryad.0cfxpnw7d

Introduction

Genomes can expand or contract through nonadaptive and adaptive mechanisms. In eukaryotes, genomes expand primarily through the self-replication of transposable elements (TEs), which produce long stretches of non-coding, repetitive DNA (Kidwell 2002; Sun et al. 2012). Genomic TE activity largely explains why genome size does not scale with the number of genes in a genome in eukaryotes (the C-value paradox; Cavalier-Smith 1978). Genome expansion may be deleterious because accumulating introns and repetitive elements could increase mutational load and mutational hazard (Lynch et al. 2006), and set lower limits to traits like cell size and the rate of cell replication (Gregory 2002). Under this view, genome expansion is a function of genetic drift, and large changes in genome size are more likely in populations where purifying selection is weak and genetic drift is strong, for example those with a small effective population size (N_e; Lynch and Conery 2003). Notably, however, the classical studies of neutral genome size evolution included data spanning prokaryotes and eukaryotes without phylogenetic correction and may have overestimated the extent to which neutral evolution can explain variation in genome size (Whitney and Garland 2010; Smith 2016).

Several adaptive hypotheses for the evolution of genome size have been proposed based on the observation that genome size correlates with several fitness-related traits, for example positively with cell size and body size, and negatively with developmental rate, developmental complexity (extent of tissue specialization), and metabolic rate (Cavalier-Smith 1982; Jockusch 1997; Kozłowski et al. 2003; Womack et al. 2019). Ecological or physiological constraints on any of these traits could lead indirectly to natural selection on genome size. For instance, miniaturization is often correlated with reductions in genome size, since cell size tends to scale positively with genome size and a minimum number of cells are required to build functional

organs (Levy and Heald 2016; Decena-Segarra et al. 2020). On the other extreme, large genomes may require other physiological accommodations, such as enucleation of red blood cells in plethodontid salamanders with especially large genomes (Mueller et al. 2008). Thus, the evolution of genome size may involve correlated changes in several traits.

Amphibians in particular are an ideal group for testing evolutionary hypotheses of genome size evolution, as they vary dramatically in genome size (Liedtke et al. 2018) and in life history traits that are correlated with genome size, such as body size, cell size, ontogeny, reproductive ecology, and metabolic rates (Gomes et al. 2004; Elinson and del Pino 2012; Levy and Heald 2016; Liedtke et al. 2022; Johnson et al. 2023). For instance, the majority of amphibians undergo an aquatic larval phase before metamorphosing into adults (Goin et al. 1968; Werner 1986; Gregory 2002), but several clades have lost the aquatic larval stage and instead undergo direct development (wherein fully formed adults develop and hatch from terrestrial eggs). Because metamorphosing species must completely reorganize their body plan within a short period of time while also facing high predation risk, they have been hypothesized to possess smaller genomes than direct-developing species (Gregory 2002). While some metamorphosing anurans do possess smaller genomes (Oeldorf et al. 1978; Lamichhaney et al. 2021), a study across Lissamphibia found no clear relationship between genome size and developmental mode (Liedtke et al. 2018). Metabolic rate, on the other hand, does appear negatively correlated with genome size across all of Lissamphibia, but this correlation breaks down when frogs or salamanders are examined independently (Licht and Lowcock 1991; Gregory 2003). Thus, among amphibians, the adaptive dynamics underlying genome size evolution may be lineage-specific and/or characterized by moderate effects of multiple independent traits, and therefore difficult to discern without denser taxon sampling at lower taxonomic levels.

In this study we characterize the extent of genome size variation in the Neotropical poison frog family Dendrobatidae (*sensu* Santos et al. [2009]), inquire on its mode of evolution, and test whether genome size is related to a suite of phenotypic traits. Three clades within Dendrobatidae have independently evolved bright coloration and the ability to sequester toxins from a diet of arthropods, along with other correlated changes, together known as the aposematic syndrome (Santos et al. 2003; Vences et al. 2003; Santos and Cannatella 2011). The evolution of chemical defense has been associated with higher aerobic capacity (Santos and Cannatella 2011), potentially related to differences in foraging strategy: toxic species tend to actively search for prey while non-toxic lineages favor a sit-and-wait strategy (Taigen and Pough 1983). Dendrobatids also exhibit substantial variation in body size (Silverstone 1975, 1976; Santos and Cannatella 2011), which, in some chemically defended species, positively correlates with defensive alkaloid quantity (Saporito et al. 2010). Thus, natural selection for chemical defense may have also indirectly resulted in genome size change by acting on either body size or metabolic rate. Because the effects of body size and metabolic rate on genome size are thought to operate in competing directions, however, the specific effects that toxicity would have on genome size are unclear.

While morphological and physiological correlates of genome size seem to oppose each other in toxic dendrobatids, another driver of genome expansion may exist at the level of molecular toxin physiology. Dendrobatid genomes appear to be on the high end of repetitive content among amphibians, commonly reaching levels above 70% (Rogers et al. 2018; Kosch et al. 2023). TE activity, which is a major determinant of genome size in vertebrates (Kidwell 2002;

Sun et al. 2012), is often regulated by Piwi-interacting RNA (piRNA; Mueller 2017) that transcriptionally silences TEs by modifying heterochromatin structure (Aravin et al. 2007). In mice, flies, nematodes and plants, the heat-shock protein *Hsp90* forms a protein complex with piwi proteins and appears critical for efficient TE suppression (Lim and Kai 2015; Specchia and Bozzetti 2021). Heat stress releases TE activity by diverting cellular *Hsp90* reservoirs towards mounting a stress response and away from TE suppression (Gangaraju et al. 2011; Piacentini et al. 2014). Whether or not *Hsp90* is involved in regulating piRNAs in frogs is currently unknown, although the piwi pathway is highly conserved in vertebrates and thus may function similarly in frogs (Lim and Kai 2015). Indeed, the smallest sequenced anuran genome, *Platyplectrum ornatum* (~1.06 Gb), has reduced TE content and increased expression of TE-suppressing Piwi genes in germline cells (Lamichhaney et al. 2021). An *in vitro* study of *Hsp90* from the liver of the poison frog *Oophaga sylvatica* was recently found to bind decahydroquinoline, an alkaloid often found in the skin of dendrobatid frogs (Daly et al. 2005), including *Oophaga sylvatica* (Caty et al. 2019). This raises the possibility of TE-driven genome expansion being facilitated by shunting *Hsp90* towards toxin binding instead of TE suppression, resulting in larger genomes.

Given the three independent origins of chemical defense in Dendrobatidae (Santos et al. 2003), this family provides an opportunity to study potential patterns of adaptive genome size evolution associated with toxicity and other correlated traits. Here, we measure and compare genome size in 34 species of dendrobatid frogs, encompassing the three chemically defended clades as well as most non-toxic lineages, to first characterize the mode of genome size evolution along the family phylogeny, and then assess whether several phenotypes, such as physiological, morphological, and life history traits, as well as environmental variables (elevation and temperature) correlate with genome size variation across Dendrobatidae. We find that genome size varies substantially within the family, likely due to fast rates of gradual evolution, as well as at most two potential punctuated rate shifts. In addition, we find that genome size correlates positively with body size, oocyte number, and clutch size, and negatively with active metabolic rate and scope, yet shows no clear relationship with toxicity or other life history attributes.

Methods

Our general approach for genome size estimation consisted of using specimens stored in the Museum of Vertebrate Zoology at the University of California, Berkeley (MVZ) to obtain red blood cells from which we quantified DNA content using Feulgen staining and computational image analysis (Feulgen microdensitometry; Hardie et al. [2002]). In addition, we produced flow cytometry estimates for four species in the genus *Phyllobates*. We then used these data to evaluate the mode of evolution of genome size and its correlates.

Specimen identification

We first reviewed the species identification for the specimens used in this study (Table S1) by examining the morphology and collection site of each specimen and comparing them to relevant literature and occurrence databases. We generated a list of dendrobatid species that occur in the country of a given specimen's collection site using the AmphibiaWeb country-specific species search (AmphibiaWeb 2023). Dendrobatid morphology is difficult to confuse with other co-occurring species, but when relevant we considered non-dendrobatids (*e.g.*,

Lithodytes lineatus, *Pristimantis* spp.) as potential misidentifications as well. We excluded from the country-specific species list any dendrobatid whose range is unlikely to overlap with the specimen collection site based on relevant literature and publicly available collection data (e.g., GBIF data imported into AmphibiaWeb's Berkeley Mapper tool). We recognize that range data present in online databases is imperfect, so when necessary we also reviewed primary literature to rule out or confirm specific identifications. We excluded any co-occurring species that could be clearly ruled out with morphological characters (according to Grant et al. [2006, 2017]) and then morphologically assessed each MVZ specimen using the dendrobatid character matrix from Grant et al. (2017) to either confirm or revise each putative ID (see Table S1 for more details).

We also reviewed the source literature for all of the collated genome size measurements of anurans in the Animal Genome Size Database (AGSD; Gregory 2022)). For non-dendrobatid anurans on AGSD, we minimally checked that the species identification listed matched with the collection site of the specimen (when data were available). For dendrobatid data published on AGSD, when possible we additionally reviewed source specimens or photographs of source specimens to confirm species identifications (see Table S2 for more details).

Cell extraction, staining, and imaging

We extracted red blood cells from formalin-fixed specimens stored in ethanol in the MVZ, and from lab-reared individuals of *Phyllobates* housed at the University of Michigan. All frog-rearing protocols were approved by the University of Michigan's Institutional Animal Care and Use Committee (protocol #PRO00010325). Cells were stained and imaged as detailed below in two separate batches. Batch one included 22 dendrobatid species and 6 non-dendrobatid species with published genome sizes (Table S2). Batch two included 10 dendrobatid species and 12 non-dendrobatid species (Table S2). For each batch we drew blood cells 4 times total from 1-2 individuals per species, deposited cells from all species arbitrarily across a set of microscope slides to prevent batch bias and allowed the cell extracts to air dry for 30 minutes. We used Feulgen staining as detailed in (Hardie et al. 2002) to stain the chromatin of dried cells. In brief, we fixed cells in 85 methanol:10 formalin:5 acetic acid for 24 hours, rinsed cells under running water for 10-minutes, hydrolyzed cells in 5.0 N HCl for 2 hours, briefly submerged cells in 0.1 N HCl, then stained cells for 2 hours with Schiff's reagent (Fisher Scientific 632-99-55). Next, we rinsed cells with bisulfite solution 3 times for 5 minutes, followed by a 10-minute wash under running water and 3 2-minute rinses in distilled water. We air-dried slides and mounted cover glass on slides using Permount (Fisher SP15500).

We imaged cells using a SeBa camera (SEBACAM5C) mounted to an Laxco LMC-2000 microscope with a 100x immersion oil lens. We white-balanced each slide individually, which sets the background color to white, using SeBa imaging software SebaView v3.7 prior to imaging.

Genome and cell size estimation

We used ImageJ v1.53c to calculate the integrated optical density (IOD) from cell images, which measures the amount of stained material (i.e., DNA), in 6-66 nuclei per species (average = 19.93 nuclei, SD = 12.18). IOD is measured in arbitrary units, but should increase linearly with DNA content per cell, and therefore genome size (Hardie et al. 2002) To convert IOD values to genome size estimates, we generated IOD measurements for 15 species with published genome sizes and four species for which we estimated genome sizes using flow

cytometry (Tables S1 and S2; see below for cytometry methods), and used them to generate a standard curve. We obtained the median IOD across nuclei for each specimen, and for species with more than one sampled specimen we obtained the median of specimen medians. Because cells were sampled, stained, and imaged in two separate batches, our standard curve consisted of a linear mixed-effects model with genome size as the dependent variable, IOD as a fixed-effect predictor, and sampling batch as a random-effect predictor. Model fitting was done using the *lmer* function of the *lme4* R package (Bates et al. 2015). Seven species were included in both staining batches to assess repeatability in genome size estimates between batches. One species (*Pseudacris nigrita*) showed considerable departures from the standard curve in preliminary analyses, so it was removed from the final calibration curve. In addition, the imaged cells from *P. terribilis* appeared morphologically abnormal and yielded IOD-based estimates that were outside of the range of our standard curve. Thus, we obtained additional genome size estimates for all *Phyllobates* species using flow cytometry (see below) and use those values in subsequent analyses.

To estimate the cell size of each species we manually traced the cell membrane of 2-22 cells per species (average = 12.30 cells, SD = 5.07) in ImageJ and calculated the area within each cell. Cell sizes were averaged by species for subsequent analysis. We note that the accuracy of our genome size estimates is dependent on the accuracy of the published C-values used to generate our standard curve.

Flow cytometry

In addition to Feulgen staining, we used flow cytometry to generate (and validate) genome size estimates for four species of the genus *Phyllobates*: *P. terribilis, P. bicolor, P, aurotaenia*, and *P. vittatus*. Captive-bred specimens were euthanized with an overdose of topical benzocaine, and muscle samples were immediately dissected and flash-frozen on dry ice, and kept frozen until further use. See above for animal care and use protocol details. Genome size was estimated as described in (Johnston et al. 2019). In brief, nuclei were released from two species that serve as standards for genome size estimates (*Drosophila virilis* [1C = 328] and *Periplaneta americana* [1C = 3303]) by combining a *D. virilis* female head and part of a *P. americana* male head in 1 ml of cold Galbraith buffer in a 2-ml Dounce and grinding with 10 gentle strokes using an A (loose) pestle. Nuclei were next released from a 1-cm^3 piece of *Phyllobates* leg or tadpole tail muscle in 25 ul of cold Galbraith buffer using 25 chops of tissue with a fresh single edged razor blade (one species at a time). The *Phyllobates* nuclei were diluted to 0.95 ml with additional cold Galbraith buffer and filtered through 45 um nylon mesh into a 1.5 mL microfuge tube along with 0.05 ml of the cold Galbraith buffer pulled from the Dounce with the nuclei from the standards. The combined nuclei from the chopped poison frog muscle and the ground *D. virilis and P. americana* standards were stained with 25 µl of propidium iodide (1 mg/ml) for 3 hours in the dark at 4 °C, after which time the mean red PI fluorescence of the stained DNA in the nuclei of the sample and standards was quantified using a CytoFlex flow cytometer (Beckman Coulter). Haploid (1C) DNA quantity was calculated as (2C sample mean fluorescence/2C standard mean fluorescence) times 328 Mbp for the *D. virilis* standard and times 3303 Mbp for the *P. americana*. The two standards produced very similar average genome size estimates, although the standard error was larger for the *D. virilis* standard. Thus, the reported 1C genome size estimate for *Phyllobates* species is based on the estimate using the *P. americana* standard. We quantified genome size for 2-5 individuals per species and used the average of individual genome sizes in further analyses. A single male *P. bicolor* individual was found to

have roughly twice the genome size as its conspecifics. This frog had noticeable deformities in some of its bones, and was unable to successfully fertilize egg clutches, which leads us to suspect it may have had an anomalous ploidy, and exclude its genome size estimate from average calculations. The raw genome size data for all individuals are provided in the Dryad repository (Data S1).

Dendrobatid phylogeny

To investigate the mode of evolution and correlates of genome size from a phylogenetic perspective, we generated a time-calibrated phylogeny for our study species. This was done by pruning the consensus tree inferred by Grant et al. (2017) so it included only the species of interest in the R package ape v5.3 (Paradis and Schliep 2019), and using sequences for one mitochondrial and five nuclear loci available in GenBank (Table S3) to convert the tree's branch lengths to time units. Because the systematics of multiple poison frog groups remain understudied, and there is good evidence for both cryptic species and species complexes (e.g. (Tarvin et al. 2017; Brown et al. 2019; de Lima Moraes et al. 2019; Márquez et al. 2020), we used tree tips and sequences from the closest available locality to the collection site of the specimens used to estimate genome size (details in Table S3).

We aligned sequences for each locus (Table S3) using MUSCLE v3.8.1551 (Edgar 2004), and chose a partitioning strategy and models of sequence evolution using PartitionFinder2 (Lanfear et al. 2016). We then ran a concatenated analysis on BEAST 2.6.5 (Bouckaert et al. 2019), setting the Grant et al. (2017) topology as a hard constraint, and using three normally-distributed calibration priors based on previous studies: The root of Dendrobatidae (i.e. the root of the tree) was set to N(μ = 38.534, σ = 5.151) following Santos et al. (Santos et al. 2009), and the nodes corresponding to Dendrobatinae and Colostethinae (*sensu* (Grant et al. 2006)) were set to N(μ=26.655, σ=4.791) and N(μ=19.392, σ=3.793), respectively, based on Guillory et al. (2019). Because one of the species for which we had a genome size estimate, *Anomaloglossus surinamensis*, was not included in Grant et al.'s (2017) phylogeny, we placed it as the sister species to *Anomaloglossus stepheni* following Vacher et al. (2017). Although *Aromobates tokuko* was recently shown to have a remarkably small genome (0.8 pg; Liedtke et al. 2018), there are no DNA sequences available for this species, so we did not include it in our analyses.

We used empirical base frequencies and a calibrated Yule tree prior (Heled and Drummond 2012), and set the Yule birth rate and clock rate priors to gamma(0.01, 50), and the GTR relative rate priors to gamma(2, 0.5) for transitions and gamma(2, 0.25) for transversions. All other priors were left at the default. Independent uncorrelated log-normal clocks were set for all partitions, and a preliminary MCMC was run for 5 million steps, sampling every 5,000. We recovered posterior distributions of the parameters describing clock rate variation among branches (ucldStdev) that leaned heavily towards zero in four of the five nuclear loci, suggesting very little rate variation at these genes, so they were modeled under a strict clock in further runs. To obtain a final tree, we ran two independent MCMC samplers for 20 million steps, sampling every 5,000, and merged their results after discarding the initial 10% of each one as burnin. Convergence and mixing within and between runs were assessed based on effective sample sizes (ESS) and trace plots using Tracer v1.7.1 (Rambaut et al. 2018). A maximum clade credibility (MCC) tree with common ancestor node heights was generated in TreeAnnotator (distributed with BEAST) and used for all downstream analyses. The xml file used as input for BEAST2,

which includes alignments and software parameters, is available on the Dryad repository for this paper.

Mode of genome size evolution

We explored the patterns of genome size evolution along the dendrobatid phylogeny by estimating rates of evolution for this trait across the tree and evaluating the evidence for distinct evolutionary regimes among clades. First, we used BAMM (Rabosky 2014) to estimate evolutionary rates of genome size evolution along the tree and over time, and assess whether discrete rate shifts occurred at specific branches. We used the R package BAMMtools (Rabosky et al. 2014) to generate priors appropriate for the temporal and taxonomic scale of our tree and phenotype, and ran BAMM for 10,000,000 steps, sampling every 5,000, for a total of 20,000 samples from the posterior, out of which we discarded 10% as burnin. From the post-burnin BAMM samples we estimated the posterior distribution for the number of rate shifts along the tree, as well as the frequency of different rate shift configurations and their associated rates of phenotypic evolution using BAMMtools.

To further examine the extent to which discrete rate shifts have shaped the evolution of genome size in dendrobatids, we used the *l1ou* R package (Khabbazian et al. 2016) to fit and rank all possible single and multi-optimum Ornstein-Uhlenbeck (OU) models of phenotypic evolution (Hansen 1997) for our tree. Models were fit using the default lasso regression approach implemented in *l1ou*, and model fit was assessed using the phylogenetically corrected Bayesian information criterion (pBIC; Khabbazian et al. 2016). To quantify the strength of support for each model, we calculated the pBIC weight (w_i for model i) as

$$w_i = \frac{\exp(-0.5\Delta_{pBIC_i})}{\sum_{k=1}^{K}\exp(-0.5\Delta_{pBIC_k})}$$

Where Δ_{pBICi} is the difference between a given model (model i) and the best model (i.e. the one with the smallest pBIC), and K is the total number of models.

Since *l1ou* only considers variations of the OU model, it can produce misleading results if this family of models is generally not a good fit for the data. Therefore, we also compared the fit of the best-fitting model from *l1ou* with other commonly used continuous trait evolution models, namely Brownian Motion (Felsenstein 1973), Early Burst (Harmon et al. 2010), Brownian motion with a trend (Harmon et al. 2008), and a White Noise model of no phylogenetic signal. For this comparison models were fit using the *fitContinuous* function of the *geiger* package (Pennell et al. 2014), and model fit was evaluated using the corrected Akaike Information Criterion (AICc), as the pBIC has not been implemented for non-OU models. The best OU model from *l1ou* fit the data better than all the other non-OU models tested (Table 1), lending credence to our results.

Correlates of genome size

We also sought to identify traits correlated with genome size, which may shed light on the processes driving genome size evolution in Dendrobatidae. We obtained data for several physiological, ecological, and life history traits from compilations available in the literature (Santos 2012; Carvajal-Castro et al. 2021); full list of traits available in Table 2). While other studies of poison frog metabolism use the term resting metabolic rate, we opt to use the term basal metabolic rate (BMR) to remain consistent with the broader literature cited herein. We

obtained elevation from the specific museum specimens used for genome size estimation when available, or the literature otherwise. We used the snout-to-vent length (SVL) as a proxy for body size, which we measured directly on adult specimens or their photographs, except for the four *Phyllobates* species used in flow cytometry, for which SVL values were pulled from the literature (Márquez et al. 2020). Finally, we scored each species as able or unable to sequester alkaloids based on data compiled by Santos, Tarvin, and O'Connell (2016). All trait data are available in Table S4. Because several traits have missing data for at least half of the species, we may not have had sufficient power to test for correlations in every case.

To assess correlations between traits and genome size, we fit univariate phylogeny-aware linear regressions using the *phylolm* R package (Tung Ho and Ané 2014). Covariance between traits due to phylogeny was modeled under the OU model with an estimated ancestral state (OUfixedRoot model). As physiological traits are tightly correlated with body mass, we added mass as a covariate in models involving metabolic rates (data were obtained from Santos [2012]). To visualize relationships between traits as well as their phylogenetic distribution we generated phylomorphospace plots (Sidlauskas 2008) using *phytools* v1.0-1 (Revell 2012).

Results

Specimen identification

We reviewed the identification of 66 specimens from the MVZ representing 38 species, including 27 species of Dendrobatidae (Table S1). Excluding six specimens whose identifications were not yet updated to new taxonomy (e.g., *Limnodynastes ornatus* is now *Platypectrum ornatum*, *Bufo cognatus* is now *Anaxyrus cognatus*, and *Elachistocleis ovalis* is a *nomen dubium* (see notes in Heyer and Liem [1976], Caramaschi [2010], Barrio-Amorós et al. [2019]), 18 (27%) of the specimens were identified incorrectly to genus, species, or both (Table S1). Many species of dendrobatid frogs are morphologically similar including some mimics (e.g., *Allobates femoralis* and *Ameerega hahneli*) and many inconspicuous species (e.g., *Colostethus*, *Hyloxalus*, *Allobates*, etc), which makes correct identification difficult especially after long-term storage in ethanol. Although we tried our best to correctly review and identify each dendrobatid specimen, we note some remaining uncertainty regarding specific specimens (see details in Table S1).

We reviewed 48 genome size estimations of 19 species published on the Animal Genome Size Database (Table S2), including 8 measurements of 8 dendrobatid species. Excluding three species whose names were incorrect because of taxonomic changes, 5 total measurements (10%) were from animals that were identified incorrectly to genus, species, or both (4 of these were dendrobatids). One (*Dendrobates femoralis*) had since been updated in VertNet as *Lithodytes lineatus* (a frog from a different family) but had not yet been updated in AGSD. With specimen photographs we were able to reassign two other samples (*Epipedobates trivittatus*, *Colostethus marchesianus*) to their correct identifications, which were both phylogenetically distant from the original identifications (*Allobates femoralis*, *Anomaloglossus* cf. *surinamensis*, respectively). We also reviewed the morphology of specimens examined in MacCulloch et al. (1996), which were assigned at the time to two morphotypes of *Epipedobates pictus* (*E.* cf. *pictus* sp. 1 and *E.* cf. *pictus* sp. 2), and since reidentified as *Ameerega hahneli* (Reynolds and MacCulloch 2012). When reviewing these specimens, two phenotypic groupings based on light and dark coloration

corresponded to the sample sizes described by MacCulloch et al. (1996); thus, we assume that *E.* cf. *pictus* sp. 1, which included 3 individuals, corresponds to lighter-colored specimens with museum numbers ROM 22797-22799 and that *E.* cf. *pictus* sp. 2, which included 5 individuals, corresponds to darker-colored specimens with museum numbers ROM 22795-22796 and ROM 22805-22807. In contrast to the re-identification by Reynolds and MacCulloch (2012), we observed that *E.* cf. *pictus* sp. 2 have a body shape more similar to *Allobates femoralis* (uniform trunk width) than *Ameerega hahneli* (pear-shaped), which is further corroborated by morphological characteristics described in (Grant et al. 2017): the *E.* cf. *pictus* sp. 2 specimens possessed Finger V length (character 5) as state 1 (reaching distal half of distal subarticular tubercle of Finger IV), yet *Ameerega hahneli* is expected to be state 0 (Finger V length surpassing distal subarticular tubercle of Finger IV). The animals assigned to *E.* cf. *pictus* sp. 1 were small and might be juveniles of the same or another species (but likely not *Ameerega hahneli*, assuming that character 5 state doesn't change with ontogeny). Thus, we tentatively reassign *E.* cf. *pictus* sp. 2 to *Allobates femoralis* but refrain from assigning a species identification for *E.* cf. *pictus* sp. 1 without further information and do not include them in our analyses.

Genome size estimation

We estimated the genome size of 32 species with previously unknown genome sizes (Table S5). Four were estimated with flow cytometry and 28 using regression coefficients from a standard curve of mean IOD vs. C-value for 18 species with known genome sizes (either previously published or measured here using flow cytometry). Median IOD of species with known genomes were tightly correlated with their genome size (Fig. S1AB), and genome size estimates were highly repeatable between imaging batches (slope = 0.92; Fig. S1C). Estimated genome sizes (C-value) across Dendrobatidae ranged from 2.6 pg (*Hyloxalus infraguttatus*) to 13.0 pg (*Phyllobates bicolor*; Fig. 1).

Based on genome size estimates and specimen identifications, we found what appears to be genome size polymorphism, extreme mimicry between *Ameerega hahneli* and *Allobates femoralis*, or cryptic species of *Am. hahneli*. We measured the genome size of two specimens from Colombia (MVZ:Herp:63120 and MVZ:Herp:63759) that were collected at the same site and are morphologically indistinguishable from each other. These two specimens are also morphologically indistinguishable from additional specimens collected at a nearby locality (UQUINDÍO:HERPETOS-UQ:ARUQ-1099–1102; Table S1) that were identified as *Am. hahneli* based on mitochondrial DNA sequences, suggesting that both MVZ specimens are likely to be *Am. hahneli*. However, we obtained notably different genome size estimates for the two MVZ specimens: 5.24 pg and 7.80 pg, respectively (Table S5). Similarly, MacCulloch et al. (1996) also reported two C-values (6.55 pg and 8.9 pg) for specimens collected in Guyana that were initially identified as *Epipedobates* cf. *pictus* sp. 1 and *E.* cf. *pictus* sp. 2. We reassigned the latter to *Allobates femoralis*, but we could not unequivocally identify the former (see Table S2 for details). Camper et al. (1993) reported the C-value of an *Allobates femoralis* specimen collected from French Guiana (previously identified as *Epipedobates trivittatus*) as 8.49 pg, similar to the value from MacCulloch et al. (1996) for *E.* cf. *pictus* sp. 2, and supporting our reassignment of *E.* cf. *pictus* sp. 2 to *Al. femoralis*. However, our measurement of such disparate values from two potential conspecifics collected at the same locality is perplexing. Three scenarios are plausible. 1) MVZ:Herp:63759 is misidentified and is actually *Al. femoralis*, suggesting that *Al. femoralis* varies in genome size (with C-values of 7.8 pg, 8.49 pg, 8.9 pg). 2)

Both MVZ specimens are identified correctly as *Am. hahneli*, suggesting that *Am. hahneli* varies moderately in genome size (with C-values of 5.24 pg and 7.8 pg). 3) The two MVZ specimens represent cryptic species with distinct genome sizes. Unfortunately, the MVZ specimens were collected in 1950 and well-preserved tissue samples are unavailable to easily verify these patterns.

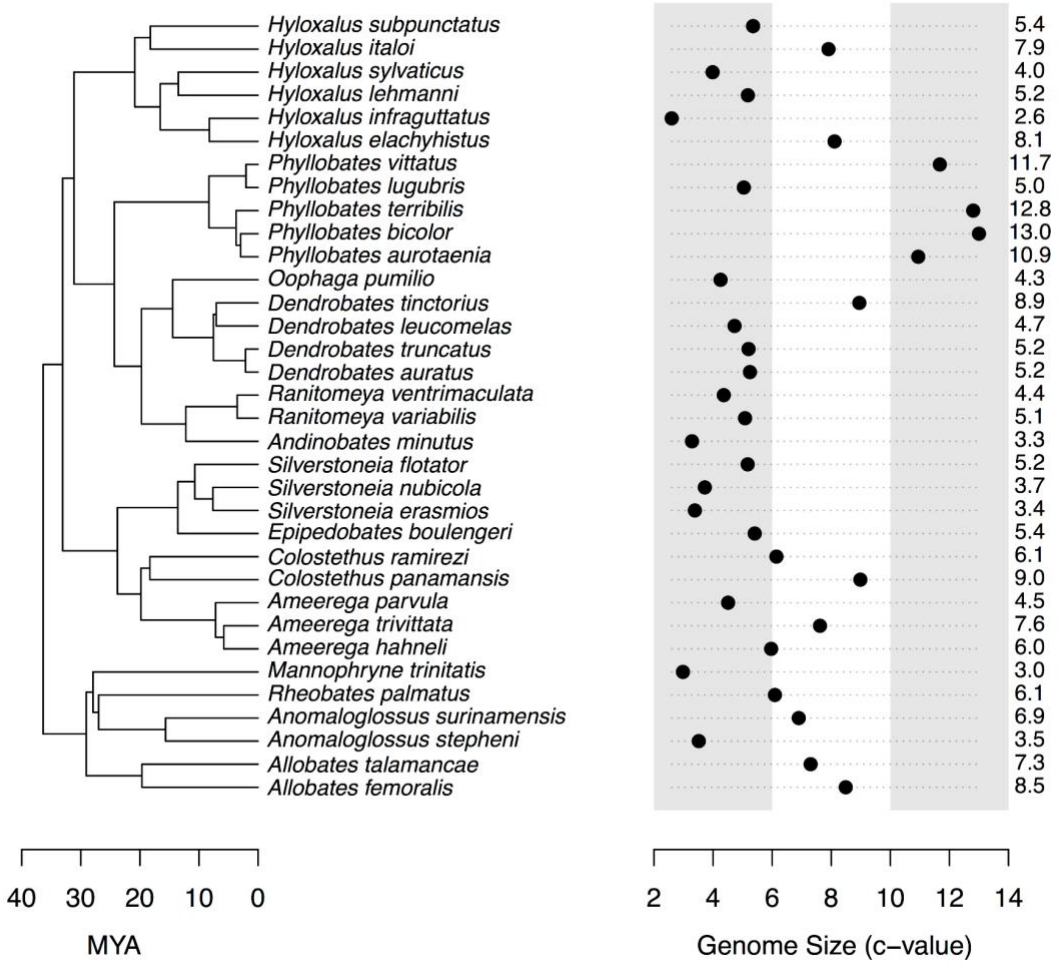

Figure 1. Genome size variation across the dendrobatid phylogeny. Numbers to the right of the dot plot represent estimated or measured genome sizes for each species. MYA: Million Years Ago.

Mode of genome size evolution

The rate of genome size evolution was relatively similar across the dendrobatid tree and stable through time, with noticeably faster rates concentrated in the branches containing the five species of *Phyllobates*, and in *Hyloxalus elachyhistus* and *H. infraguttatus* (Fig 2AB). Both BAMM and *l1ou* showed some evidence that this variation is due to discrete rate shifts at these branches, since the posterior distribution for the number of rate shifts recovered by BAMM peaked at 1-2 shifts (Fig. 2B), and the top rate configurations from both BAMM and *l1ou* analyses contained scenarios with 1-2 rate shifts along the branches mentioned above (Figs. 3, S3, S4). However, models with no rate shifts were also strongly supported by both analyses (Fig.

3BF), indicating that despite faster genome size evolution, the branches in question may just represent data points from the edges of a single evolutionary rate distribution. Our current data do not allow us to distinguish between both scenarios.

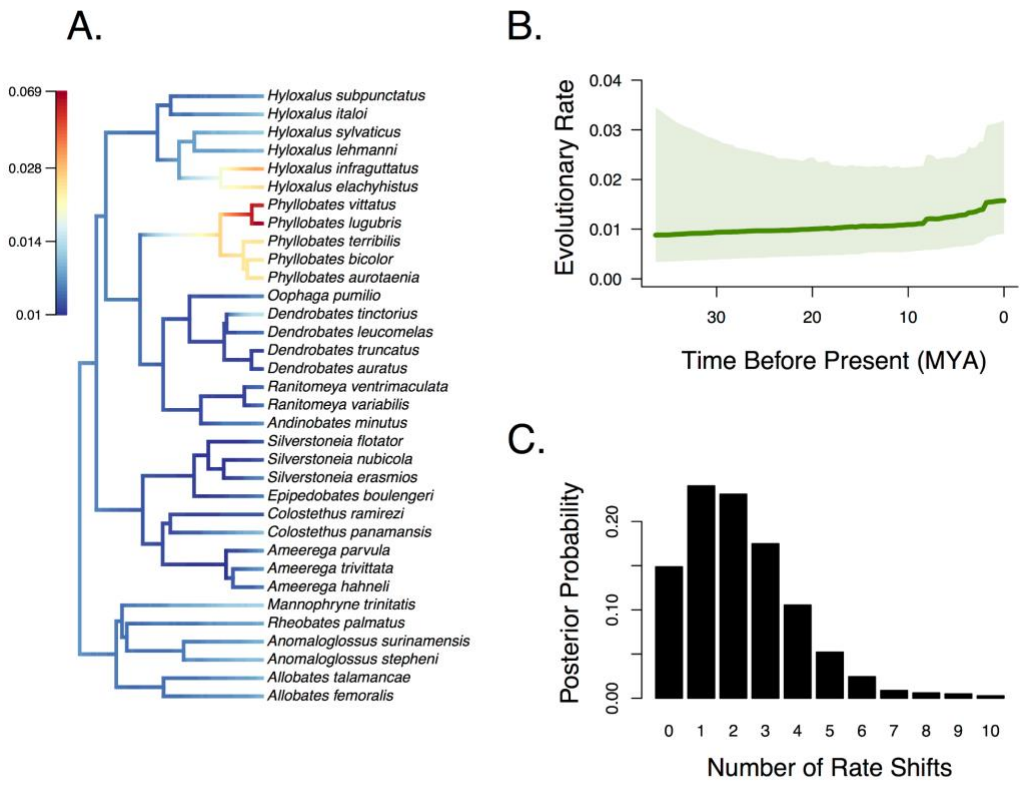

Figure 2. Rate of genome size evolution in dendrobatid frogs. A) Instantaneous rates of phenotypic evolution along the dendrobatid phylogeny and B) across the phylogeny over time. C) Posterior distribution of the number of discrete rate shifts recovered by BAMM. The color ramp in panel A was generated using the Jenks method in the plot.bammdata() function of BAMMtools. Panel B is based on 100 time slices, the central line depicts the median posterior rate, and the surrounding polygon the 95% highest posterior density.

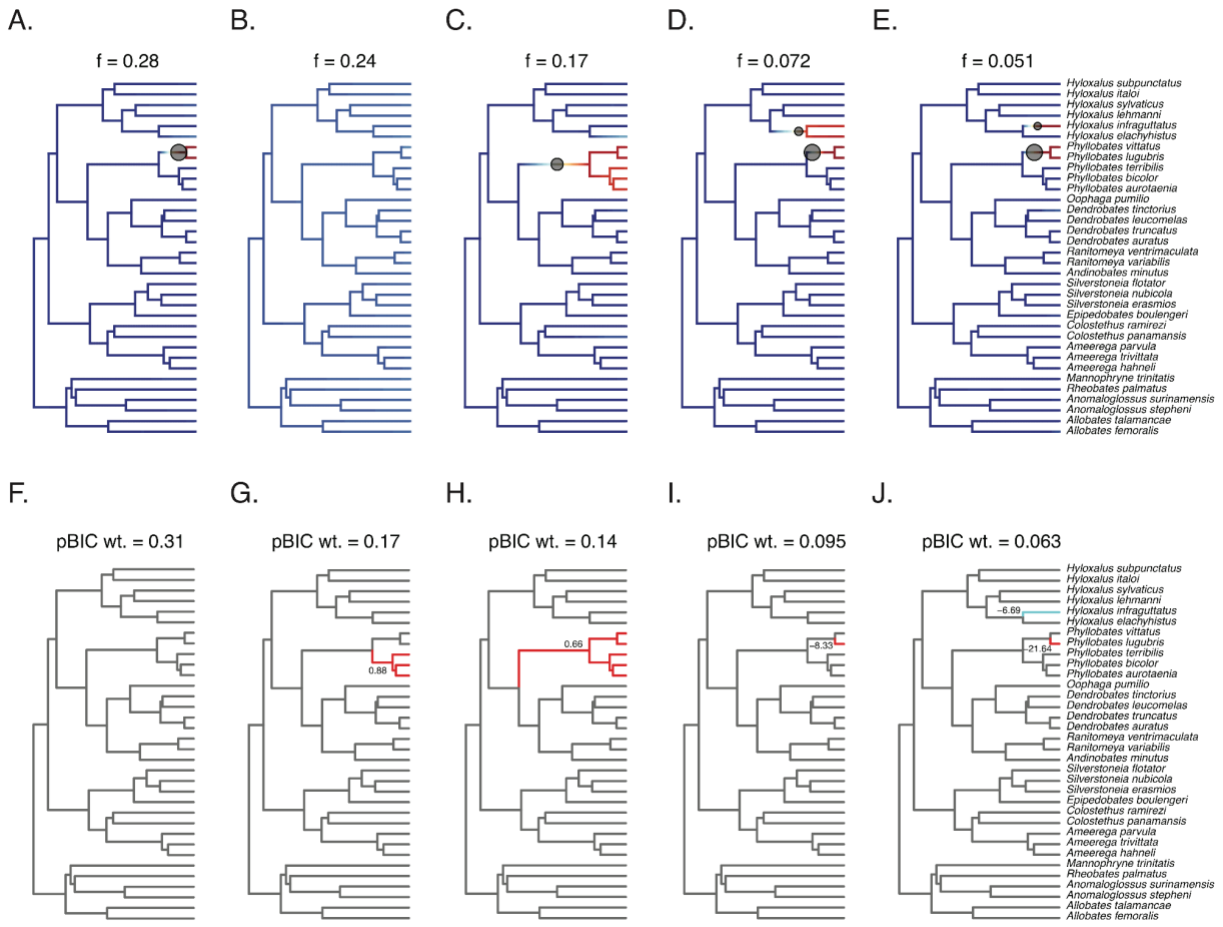

Figure 3. Evidence for discrete shifts in genome size evolution. Panels A-E show the five most frequent rate shift configurations in the BAMM posterior output along with their posterior probabilities. Circles mark positions of rate shifts, with sizes proportional to marginal shift probability. Warmer colors represent faster evolutionary rates. These configurations account for 81.3% of the posterior density. Figure S3 depicts the 9 configurations that make up 95% of the posterior density. Panels F-J show the five best-fitting multi-regime OU models from *l1ou* and their pBIC weights. Clades are colored by OU regime, and branch numbers indicate the magnitude of each estimated regime shift. These models correspond to 78% of the pBIC weight among all tested models. Figure S4 contains the top 12 models, corresponding to 90% of the pBIC weight.

Correlates of genome size

Six of the 15 tested traits were correlated with genome size (Table 2). Body size, oocyte number, clutch size, and cell area showed positive correlations with genome size. Active metabolic rate (AMR) and aerobic scope were negatively correlated with genome size even after controlling for body mass and phylogeny. Basal metabolic rate (BMR) was, however, not correlated with genome size after controlling for mass. Since the aerobic scope measures the difference between active and basal metabolic rates, this suggests that the correlation between scope and genome size is driven mainly by the active metabolic rate. Because some species of *Phyllobates* were outliers in terms of genome size and some of the tested predictors, we re-ran our linear regressions excluding this genus from the dataset. The results from the full dataset were qualitatively the same, albeit with lower effect sizes and weaker statistical significance.

Model fitting results for the 15 predictors, both with and without *Phyllobates*, are given in Table 2, and Figure 4 shows the relationships between genome size and the six correlated predictors.

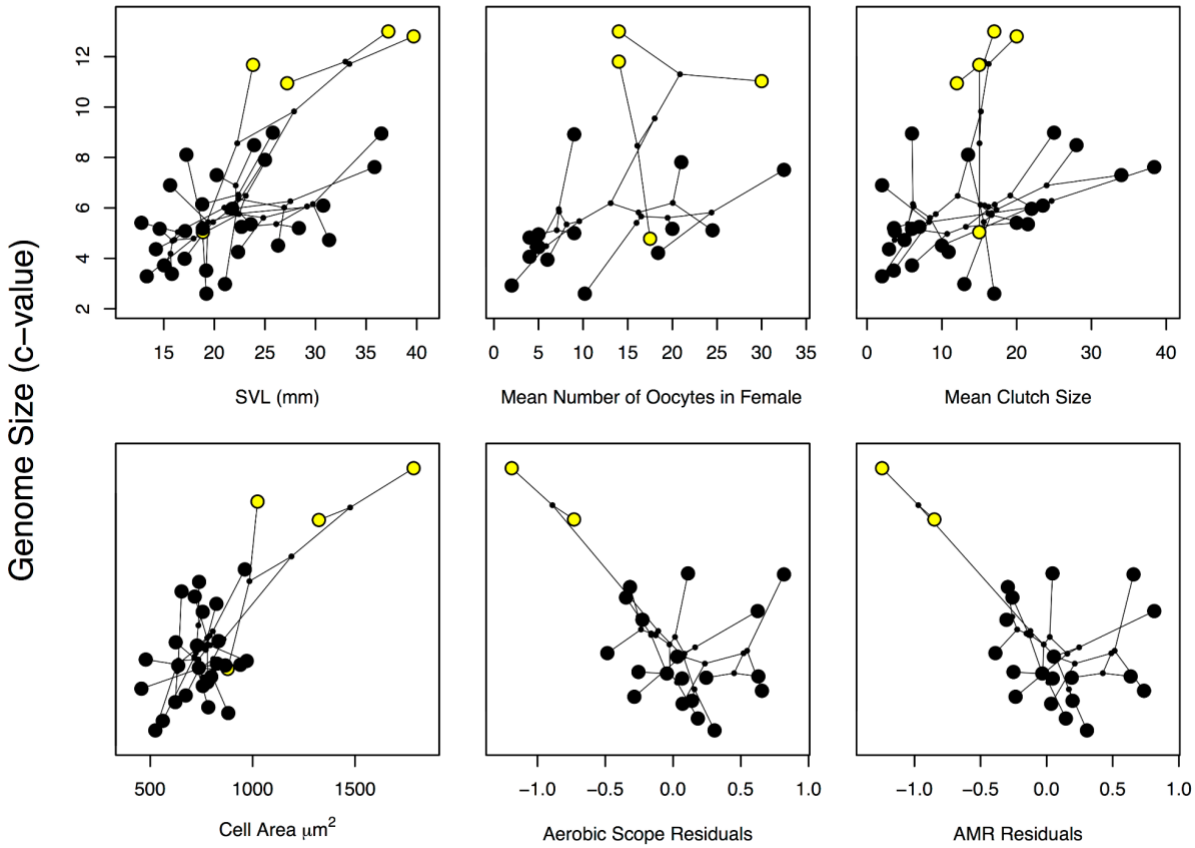

Figure 4. Phylomorphospace plots of the relationships between genome size and the six predictors that showed significant correlations. Large dots represent extant species, connected by lines that depict phylogeny. Small dots indicate bivariate ancestral state reconstructions. Species in the genus *Phyllobates* are colored yellow and all others black. For the two metabolic variables (aerobic scope and AMR) we plot the linear residuals with mass instead of the raw values to provide a visualization that controls for body mass. For model fitting mass was used as a covariate instead.

Discussion

Genome size evolution in Dendrobatidae

Dendrobatid genome sizes vary across the full range characterized in Anura, with a minimum C-value of 0.8 pg (*Aromobates tokuko*) and a maximum value of 13.0 pg (*Phyllobates bicolor*). In addition to *A. tokuko* having the smallest reported frog genome (Liedtke et al. 2018), *Phyllobates bicolor* and *P. terribilis* now rank as the first and second largest published anuran genomes to date, outsizing *Bombina bombina* with an average C-value of 11.38 pg (Liedtke et al. 2018; Gregory 2022). The greater than ten-fold variation in genome size among dendrobatids is broader than what has been observed in the few other similarly well-sampled amphibian families, such as plethodontid salamanders with a 5.2-fold range (13.90 – 71.65 pg; N = 95 species), hylid tree frogs with a 4.3-fold range (1.54 – 6.61 pg; N = 41 species), or bufonid toads with a 2.5-fold

range (2.91 – 7.31 pg; N = 31 species). Given the lack of comprehensive phylogenetic sampling in these and other families, we expect that additional cases of broad variation in genome size at lower taxonomic scales among amphibians will be described in the future.

The fact that dendrobatids have occupied the entire genome size range covered by frogs in just under 40 million years may be explained by their much faster rate of genome size evolution (Fig 2B) compared to the average rates across all frogs and other amphibian orders, which are over one order of magnitude lower (Liedtke et al. 2018). Previous work suggests that, across amphibians, genome size has evolved in a mostly gradual manner, with only a few saltational genome size shifts (Liedtke et al. 2018). Our results, which focused on a shallower phylogenetic scale, point to a similar scenario. We find strong evidence that most, if not all branches of the dendrobatid phylogeny have evolved under the same gradual evolutionary regime. We also find some evidence of one or two discrete rate shifts, although we recognize that the evidence is statistically ambiguous, and these putative shifts could also just represent clades at the extremes of the distribution of this quickly evolving trait under a single regime scenario. In any case, these results further point to the accumulation of small-effect events, such as gradual TE amplification or suppression, as the main mechanisms underlying genome size evolution in amphibians, as opposed to large-effect events, such as the duplication/loss of large genomic regions, or short-lived explosive bursts of TE amplification.

Phenotypic data suggest that at least one of the putative discrete genome size shifts detected may be biologically realistic. Species in the genus *Phyllobates* display a suite of other phenotypic correlates of genome size visibly outside the range of other dendrobatids, including categorically lower active and basal metabolic rates and aerobic scopes than expected given their mass, as well as much larger cell areas than other dendrobatid species (Fig. 4). *Phyllobates* frogs likely represent an independent evolutionary origin of aposematism (Grant et al. 2017), marked by the ability to sequester batrachotoxin (Myers et al. 1978), a potent neurotoxin potentially unique to *Phyllobates* among amphibians (Daly et al. 2005; Santos et al. 2016). Whether this transition to aposematism and the observed genome size shift are mechanistically connected or coincidentally occurred along the same branch of the phylogeny remains to be determined.

Phenotypic correlates of genome size

We identified a significant correlation between genome size and five fitness-related traits: active metabolic rate (AMR), metabolic scope, snout-vent length (SVL), number of oocytes, and clutch size. Amongst these correlates, all but AMR and scope were positively correlated with genome size. AMR and scope are thought to be positively associated with chemical defense evolution (Santos and Cannatella 2011), while body size may be of particular significance in poison frogs because it positively correlates with toxicity, bright coloration, and mating call complexity (Saporito et al. 2010; Santos and Cannatella 2011; Santos et al. 2014; Márquez et al. 2020). Thus, we initially hypothesized that natural selection imposed by predators for greater toxin load or brighter coloration may drive increased body size and lower metabolic rate and indirectly influence genome size evolution. However, we did not find any evidence of a relationship between alkaloid sequestration and genome size. Given that AMR, scope, and SVL were correlated with genome size across our entire dataset of toxic and non-toxic species, even when toxicity is included as a covariate (Table S6), our data suggest that these traits' effects on genome size are unrelated to the evolution of chemical defense.

The mechanistic link between genome size and metabolic rate is unclear, although it has been suggested to be mediated through cell size (Cavalier-Smith 1982; Gregory 2001). Specifically, larger cells divide less frequently and have a higher surface-area-to-volume ratio and thus a slower rate of nutrient and gas exchange, both of which should decrease metabolic rate (Gregory 2001). If biophysical properties of cells are the primary determinant of the relationship between metabolic rate and genome size, we might expect the scaling relationship between metabolic rate and genome size to be biologically universal. However, this pattern is not consistent across taxa. A negative correlation between genome size and basal metabolic rate (BMR) has been observed multiple times in birds and mammals (Vinogradov 1995; Gregory 2002; Kozłowski et al. 2003), and a negative correlation between genome size and BMR has been observed across all of Lissamphibia, but not when Anura and Caudata are considered independently (Gregory 2003). In addition, AMR and genome size are negatively correlated in salamanders, but only at stress-inducing temperatures (Licht and Lowcock 1991) and ploidy level and AMR are negatively correlated in tadpoles but not froglets of the hybridogenetic frog *Pelophylax esculentus* (Hermaniuk et al. 2017). Finally, genome size does not appear to be associated with evolutionary saltations in BMR across extant vertebrates (Gardner et al. 2020), although there are exceptions in certain mammalian lineages (Uyeda et al. 2017). While AMR was not considered in some of these studies, potentially due to lack of data availability, our observation that AMR and metabolic scope are negatively correlated with genome size (controlling for mass) is fairly novel amongst amphibians. Dendrobatids in general exhibit highly specialized life history and physiology, including significant investment in parental care, coloration, toxin sequestration, and diet. Additionally, AMR (but not BMR) is positively correlated with molecular evolution rate in Dendrobatidae (Santos 2012). Thus, dendrobatids as a system may present an opportunity to clarify the mechanistic link between genome size and metabolic rate.

Similarly to metabolic rate, the positive correlation between body size and genome size is thought to be mediated through cell size, and, additionally, through cell number (Arendt 2007; Hessen et al. 2013). While the mechanism underlying the relationship between genome size and cell size remains unclear, it may be driven by variation in transcriptional output or stoichiometric relationships between DNA amount and cytoplasmic protein levels (Mueller 2015). Cell size is positively correlated with SVL in our data set (Table S6), suggesting that cell size could mediate the positive correlation between body size and genome size in poison frogs. In smaller species that have relatively large genomes for their size compared to other vertebrates (e.g., *Ranitomeya*: 4.4 – 6.8 pg, Table S5 and Stuckert et al. [2021]), cell size could limit cell number and constrain morphological complexity (i.e., biological size), as has been seen in other amphibians (Levy and Heald 2016; Womack et al. 2019; Decena-Segarra et al. 2020). One potential consequence of miniaturization is reduced complexity of the visual nervous system and hindering of vision-based behaviors such as active foraging, as has been observed in salamanders that have very large genomes (>30 pg; Roth [1990]). Given that some dendrobatids are diet specialists that actively forage for ants and mites, and that this behavior is a putative driver of chemical defense evolution, such a loss would be of particular consequence in Dendrobatidae (Toft 1995; Santos and Cannatella 2011). Furthermore, visual communication is thought to play an important role in several aspects of poison frog biology (e.g., Summers et al. [1999]; Pröhl [2005]; Yang et al. [2019]). Thus, natural selection for the maintenance of body structures used in vision could play a role in genome size reduction in some dendrobatid species. We note, however, that the genera with the smallest genomes in our dataset, *Hyloxalus* and *Anomaloglossus*, are neither

miniaturized, brightly colored, nor outliers with respect to AMR (a correlate of active foraging) (Santos and Cannatella 2011), thus we do not find strong support for this dynamic amongst the lineages we sampled.

The positive correlation we identified between fecundity and genome size is intriguing to consider in light of non-adaptive mechanisms of genome expansion, which postulate that expansion is driven by effective population size (N_e) and thus, presumably, variation in fecundity. Specifically, in populations with highly fecund individuals, a relatively small number of females could make an outsized contribution to the genetic pool and thus shrink N_e (Hedgecock 1994; Hedrick 2005). Fecundity in some vertebrate taxa allometrically scales with female body size (Shine and Greer 1991). We only observed a non-significant, positive trend between snout-vent length (SVL) and clutch size in our dataset. In some dendrobatid species, parents invest heavily in only a few offspring at a time, which might disrupt the allometric relationship that would otherwise be expected between clutch size and body size (Carvajal-Castro et al. 2021). Therefore, the positive correlation we observed between fecundity and genome size may be independent of body size and leaves room for the possibility that fecundity is positively correlated with genome size due to changes in effective population size. While beyond the scope of our study, we note that broader phylogenetic studies of fecundity, N_e and genome size may help inform the contribution of neutral processes to genome size evolution.

Accuracy of taxonomic identification in public databases

A meaningful proportion of data in each of the databases we used (10% in AGSD, 27% in MVZ) was found to be associated with an incorrect or putatively incorrect species identification (all identifications for specimens included in this paper will be updated in AGSD and MVZ during the review process). We caution and encourage users of public data to take the time to validate species identifications. Validation may be especially necessary when organisms were collected by scientists that are not experts in the focal taxon, when the specimen identifications have not been revised for several decades, and for taxa with large amounts of morphologically similar taxa. All three of these criteria apply to the MVZ dendrobatid specimens. The prevalence of misidentified specimens in databases is not new or surprising (Szczęsny and Godunko 2007; Mulcahy et al. 2022). DNA barcoding is one approach that can validate museum specimen identifications (Hebert et al. 2003), though it may not always be accurate if genetic structure at the used marker(s) does not correlate perfectly with species identity (Chambers and Hebert 2016; Mulcahy et al. 2022). Digitizing collections can also accelerate the process of validating identifications by increasing access to specimens (Cook et al. 2014).

Conclusion

The drivers of genome size evolution in eukaryotes remain a field of active research in evolutionary biology. Our results show that in dendrobatid poison frogs, genome size has evolved at much faster rates than in other amphibians — to the point of encompassing the entire range of genome sizes observed across anurans. Phylogenetic analyses suggest that this rapid evolution has proceeded primarily in a gradual manner and at a constant rate, with rare but appreciable events of punctuated evolution, although evidence for the latter is ambiguous. Correlations between genome size and life history traits suggest that cell size may mediate

changes in genome size within the group. Mechanisms underlying the relationship between cell size, metabolic rate, and genome size are not well understood, yet wide variation in each of these traits in Dendrobatidae could make the group suitable to provide mechanistic insight. Together these patterns suggest roles both for adaptive and neutral processes in shaping genome size evolution in Dendrobatidae. Our study contributes to understanding the multidimensional drivers of genome size, and sets the stage for future investigation into mechanisms driving genome size evolution in vertebrates.

Data Accessibility

Raw data files, R script and detailed metadata are available for download from the Dryad Digital Repository http://doi.org/10.5061/dryad.0cfxpnw7d.

Table Legends

Table 1. Fit of various models of continuous trait evolution to genome size data in Dendrobatidae. Models are ranked based on AICc weight.

Table 2. Phylogenetically-aware linear regression coefficients of genome size against 15 morphological, metabolic, and life history traits, including or excluding species in the genus *Phyllobates*. Body mass was included as a covariate in models involving metabolic rates.

Supplementary Material

Table S1. Specimens used for genome size estimation, with notes on revised species identifications and other specimen-specific information.

Table S2. Published C-values used in analyses and/or in our standard curve, with notes on revised species identifications. Some specimens that were not used in this study but whose identification was updated are also included.

Table S3. Genbank numbers for sequences used to time-calibrate the phylogeny used in analyses.

Table S4. Morphological, life history, and metabolic data used in regression analyses models. Life history data were obtained from Carvajal-Castro et al. (2021), metabolic and body weight data were obtained from Santos (2012), alkaloid data from Santos et al (2016), and morphological data were measured on museum specimens (see Table S1), or obtained from the literature (see Methods for details).

Table S5. Genome size estimates for each species obtained using a standard curve estimated using a linear mixed-effects model with genome size as the dependent variable, integrated optical density as a fixed-effect predictor, and sampling batch as a random-effect predictor (see Methods and Fig. S1).

Table S6. Phylogenetically-aware linear regression coefficients of genome size against 15 morphological, metabolic, and life history traits, including toxicity as a correlate. Body mass was included as a covariate in models involving metabolic rates.

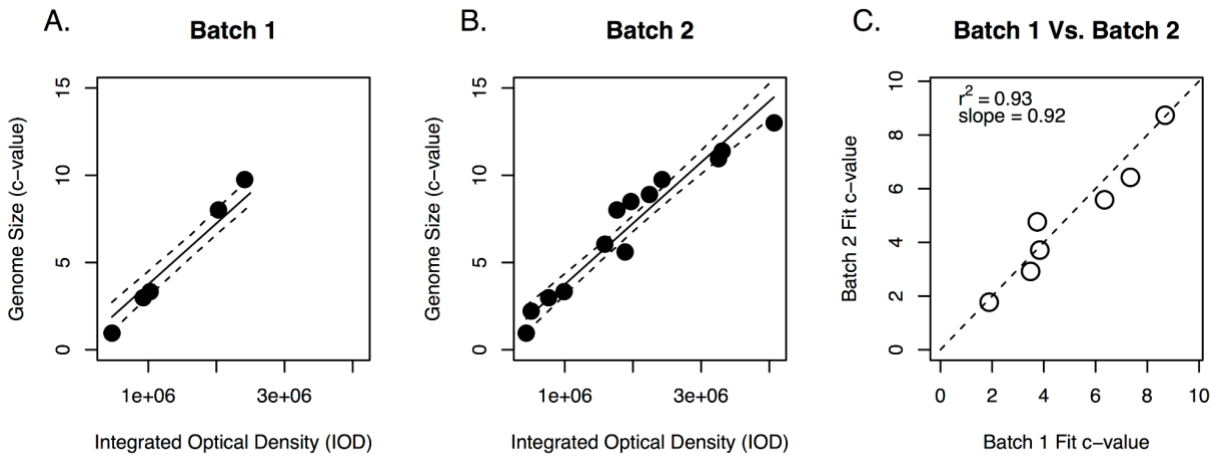

Figure S1. Standard curves used to convert IOD values to genome sizes. Panels A and B represent the curves inferred for each independent imaging batch. Solid lines represent the slope and intercept for each specific batch and broken lines 95% confidence intervals. Panel C shows genome size estimates for the seven species that were imaged in both batches. The diagonal represents the identity line.

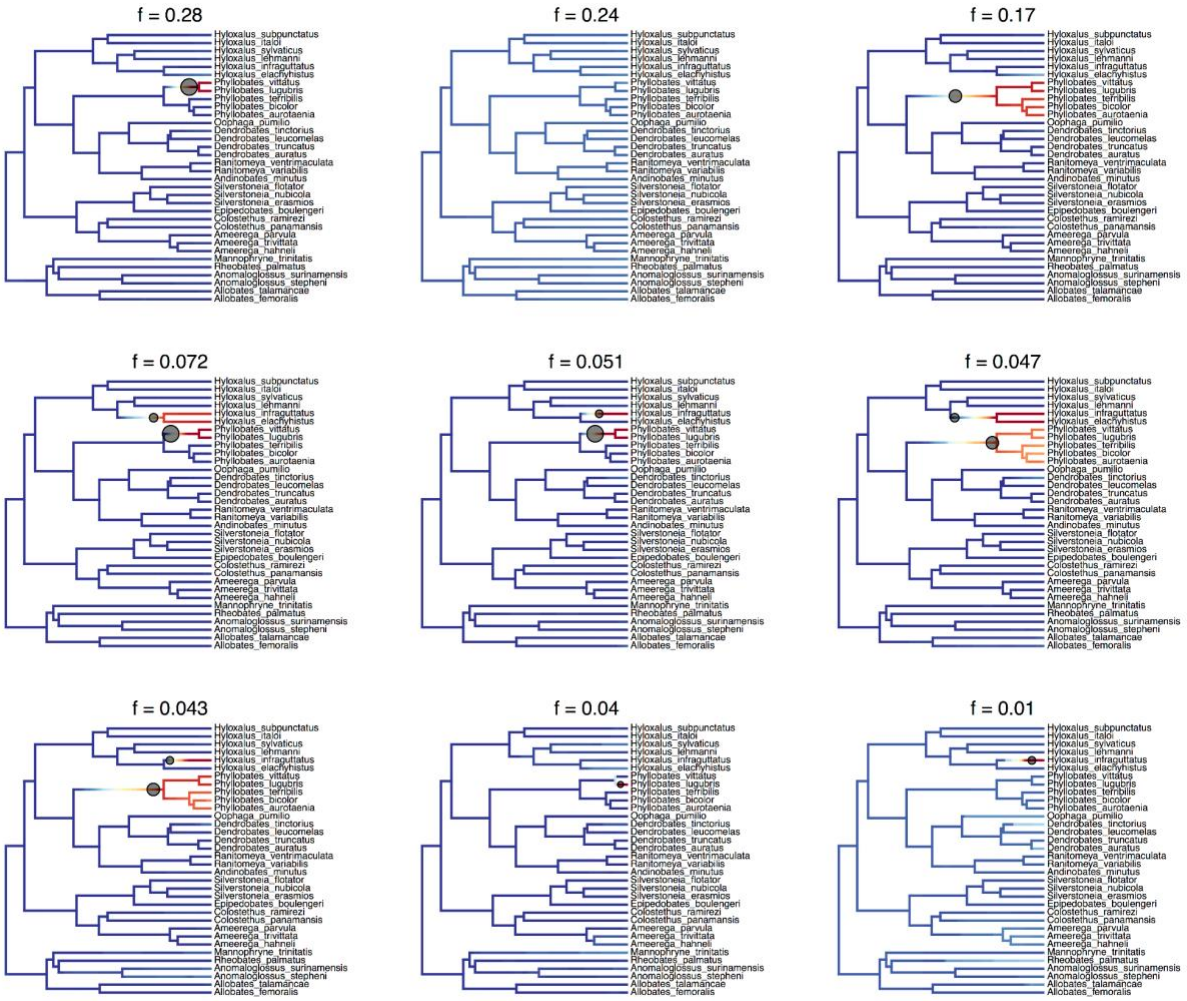

Figure S2. Top 9 BAMM shift configurations, accounting for the 95% highest posterior density. Colors and dots are as in Figure 3.

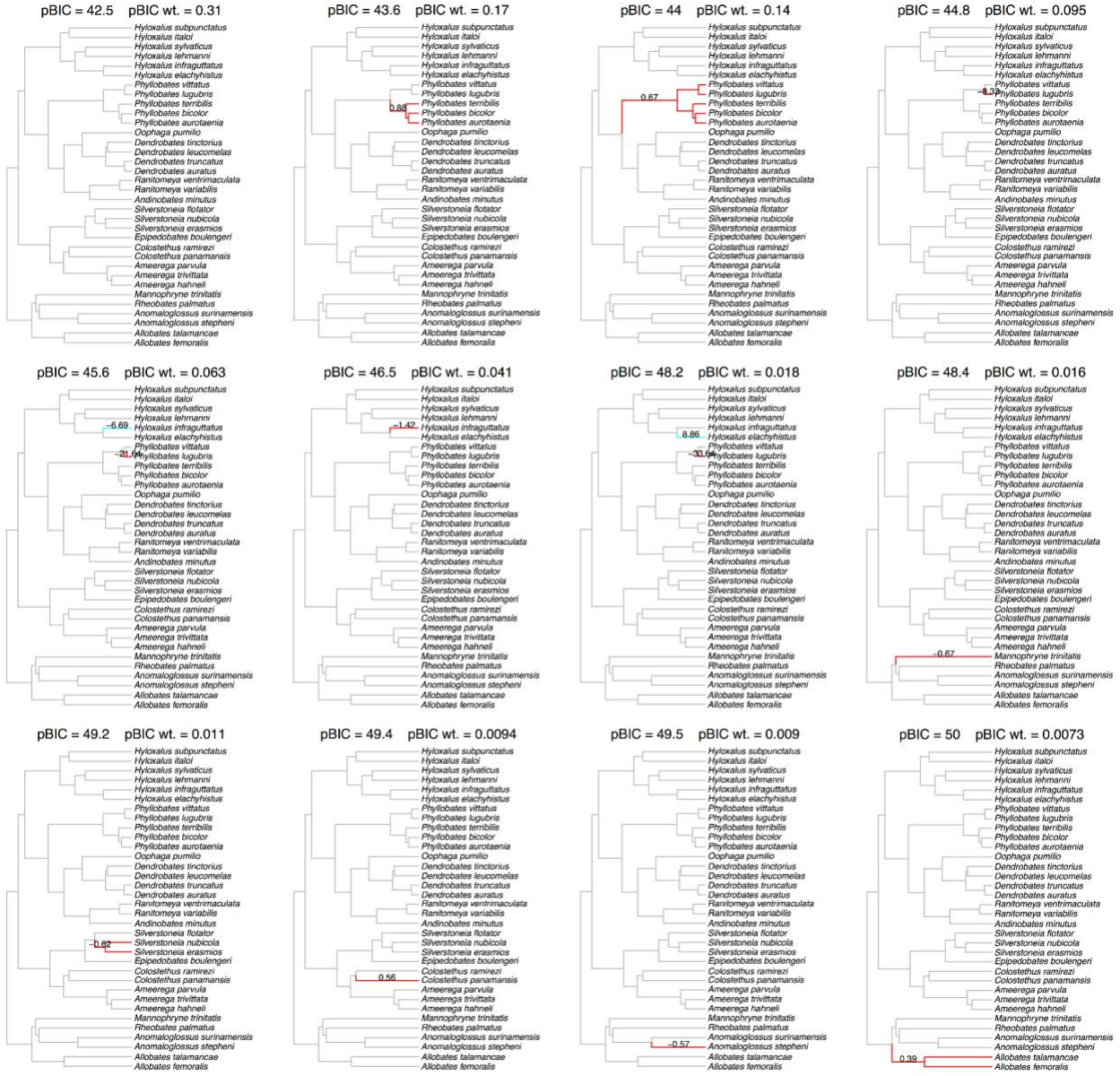

Figure S3. Top 12 multi-regime OU models fit with *l1ou*, making up 90% of the pBIC weight across the 283 possible rate shift configurations. Colors and labels are as in Figure 3.

References

AmphibiaWeb. 2023. University of California, Berkeley, CA, USA.

Aravin, A. A., G. J. Hannon, and J. Brennecke. 2007. The Piwi-piRNA pathway provides an adaptive defense in the transposon arms race. Science 318:761–764.

Arendt, J. 2007. Ecological correlates of body size in relation to cell size and cell number: patterns in flies, fish, fruits and foliage. Biological Reviews 82:241–256.

Barrio-Amorós, C. L., F. J. M. Rojas-Runjaic, and J. Celsa Señaris. 2019. Catalogue of the amphibians of Venezuela: Illustrated and annotated species list, distribution, and conservation. Amphibian & Reptile Conservation 13:200.

Bates, D., M. Mächler, B. Bolker, and S. Walker. 2015. Fitting linear mixed-effects models using lme4. Journal of Statistical Software 67.

Bouckaert, R., T. G. Vaughan, J. Barido-Sottani, S. Duchêne, M. Fourment, A. Gavryushkina, J. Heled, et al. 2019. BEAST 2.5: An advanced software platform for Bayesian evolutionary analysis. PLOS Computational Biology 15:e1006650.

Brown, J. L., K. Siu-Ting, R. Von May, E. Twomey, W. X. Guillory, M. S. Deutsch, and G. Chávez. 2019. Systematics of the *Ameerega rubriventris* complex (Anura: Dendrobatidae) with descriptions of two new cryptic species from the East-Andean versant of Peru. Zootaxa 4712:211–235.

Camper, J. D., L. A. Ruedas, J. W. Bickham, and J. R. Dixon. 1993. The relationship of genome size with developmental rates and reproductive strategies in five families of Neotropical bufonid frogs. Life Science Advances -- Genetics 12:79–87.

Caramaschi, U. 2010. Notes on the taxonomic status of *Elachistocleis ovalis* (Schneider, 1799) and description of five new species of *Elachistocleis* Parker, 1927 (Amphibia, Anura, Microhylidae). Boletim do Museu Nacional Rio de Janeiro Zoologia 527:1–30.

Carvajal-Castro, J. D., F. Vargas-Salinas, S. Casas-Cardona, B. Rojas, and J. C. Santos. 2021. Aposematism facilitates the diversification of parental care strategies in poison frogs. Scientific Reports 11:19047.

Caty, S. N., A. Alvarez-Buylla, G. D. Byrd, C. Vidoudez, A. B. Roland, E. E. Tapia, B. Budnik, et al. 2019. Molecular physiology of chemical defenses in a poison frog. Journal of Experimental Biology 222:jeb204149.

Cavalier-Smith, T. 1978. Nuclear volume control by nucleoskeletal DNA, selection for cell volume and cell growth rate, and the solution of the DNA C-value paradox. Journal of Cell Science 34:247–278.

Cavalier-Smith, T. 1982. Skeletal DNA and the evolution of genome size. Annual Review of Biophysics and Bioengineering 11:273–302.

Chambers, E. A., and P. D. N. Hebert. 2016. Assessing DNA barcodes for species identification in North American reptiles and amphibians in natural history collections. PLOS ONE 11:e0154363.

Cook, J. A., S. V. Edwards, E. A. Lacey, R. P. Guralnick, P. S. Soltis, D. E. Soltis, C. K. Welch, et al. 2014. Natural history collections as emerging resources for innovative education. BioScience 64:725–734.

Daly, J. W., T. F. Spande, and H. M. Garraffo. 2005. Alkaloids from amphibian skin: A tabulation of over eight-hundred compounds. Journal of Natural Products 68:1556–1575.

de Lima Moraes, L. J. C., D. Pavan, and A. P. Lima. 2019. A new nurse frog of *Allobates masniger-nidicola* complex (Anura, Aromobatidae) from the east bank of Tapajós River, eastern Amazonia. Zootaxa 4648:401–434.

Decena-Segarra, L. P., L. Bizjak-Mali, A. Kladnik, S. K. Sessions, and S. M. Rovito. 2020. Miniaturization, Genome Size, and Biological Size in a Diverse Clade of Salamanders. The American Naturalist 196:634–648.

Edgar, R. C. 2004. MUSCLE: multiple sequence alignment with high accuracy and high throughput. Nucleic Acids Research 32:1792–1797.

Elinson, R. P., and E. M. del Pino. 2012. Developmental diversity of amphibians. WIREs Developmental Biology 1:345–369.

Felsenstein, J. 1973. Maximum-likelihood estimation of evolutionary trees from continuous characters. American Journal of Human Genetics 25:471–492.

Gangaraju, V. K., H. Yin, M. M. Weiner, J. Wang, X. A. Huang, and H. Lin. 2011. *Drosophila* Piwi functions in Hsp90-mediated suppression of phenotypic variation. Nature Genetics 43:153–158.

Gardner, J. D., M. Laurin, and C. L. Organ. 2020. The relationship between genome size and metabolic rate in extant vertebrates. Philosophical Transactions of the Royal Society B: Biological Sciences 375:20190146.

Goin, O. B., C. J. Goin, and K. Bachmann. 1968. DNA and amphibian life history. Copeia 532.

Gomes, F. R., J. Guilherme Chauí-Berlinck, J. E. P. W. Bicudo, and C. A. Navas. 2004. Intraspecific relationships between resting and activity metabolism in anuran amphibians: Influence of ecology and behavior. Physiological and Biochemical Zoology 77:197–208.

Grant, T., D. R. Frost, J. P. Caldwell, R. Gagliardo, C. F. B. Haddad, P. J. R. Kok, D. B. Means, et al. 2006. Phylogenetic systematics of dart-poison frogs and their relatives (Amphibia: Athesphatanura: Dendrobatidae). Bulletin of the American Museum of Natural History 299:1–262.

Grant, T., M. Rada, M. Anganoy-Criollo, A. Batista, P. H. Dias, A. M. Jeckel, D. J. Machado, et al. 2017. Phylogenetic systematics of dart-poison frogs and their relatives revisited (Anura: Dendrobatoidea). South American Journal of Herpetology 12.

Gregory, T. R. 2001. Coincidence, coevolution, or causation? DNA content, cell size, and the C-value enigma. Biological Reviews 76:65–101.

———. 2002. Genome size and developmental complexity. Genetica 115:131–146.

———. 2003. Variation across amphibian species in the size of the nuclear genome supports a pluralistic, hierarchical approach to the C-value enigma. Biological Journal of the Linnean Society 79:329–339.

———. 2022. Animal Genome Size Database.

Guillory, W. X., M. R. Muell, K. Summers, and J. L. Brown. 2019. Phylogenomic reconstruction of the Neotropical poison frogs (Dendrobatidae) and their conservation. Diversity 11:126.

Hansen, T. F. 1997. Stabilizing selection and the comparative analysis of adaptation. Evolution 51:1341–1351.

Hardie, D. C., T. R. Gregory, and P. D. N. Hebert. 2002. From pixels to picograms: A beginners' guide to genome quantification by Feulgen image analysis densitometry. The Journal of Histochemistry and Cytochemistry 50:735–749.

Harmon, L. J., J. B. Losos, T. Jonathan Davies, R. G. Gillespie, J. L. Gittleman, W. Bryan Jennings, K. H. Kozak, et al. 2010. Early bursts of body size and shape evolution are rare in comparative data. Evolution 64:2385–2396.

Harmon, L. J., J. T. Weir, C. D. Brock, R. E. Glor, and W. Challenger. 2008. GEIGER: investigating evolutionary radiations. Bioinformatics 24:129–131.

Hebert, P. D. N., A. Cywinska, S. L. Ball, and J. R. deWaard. 2003. Biological identifications

through DNA barcodes. Proceedings of the Royal Society of London. Series B: Biological Sciences 270:313–321.
Hedgecock, D. 1994. Does variance in reproductive success limit effective population sizes of marine organisms? Pages 122–134 *in*Genetics and Evolution of Aquatic Organisms, A. R. Beaumont (Ed.). Chapman & Hall, London.
Hedrick, P. 2005. Large Variance in Reproductive Success and the N_e/N Ratio. Evolution 59:1596–1599.
Heled, J., and A. J. Drummond. 2012. Calibrated tree priors for relaxed phylogenetics and divergence time estimation. Systematic Biology 61:138–149.
Hermaniuk, A., M. Rybacki, and J. R. E. Taylor. 2017. Metabolic rate of diploid and triploid edible frog *Pelophylax esculentus* correlates inversely with cell size in tadpoles but not in frogs. Physiological and Biochemical Zoology 90:230–239.
Hessen, D. O., M. Daufresne, and H. P. Leinaas. 2013. Temperature-size relations from the cellular-genomic perspective. Biological Reviews 88:476–489.
Heyer, W. R., and D. S. Liem. 1976. Analysis of the intergeneric relationships of the Australian frog family Myobatrachidae. Smithsonian Contributions to Zoology 233:1–29.
Jockusch, E. L. 1997. An evolutionary correlate of genome size change in plethodontid salamanders. Proceedings of the Royal Society of London. Series B: Biological Sciences 264:597–604.
Johnson, J. V., C. Finn, J. Guirguis, L. E. B. Goodyear, L. P. Harvey, R. Magee, S. Ron, et al. 2023. What drives the evolution of body size in ectotherms? A global analysis across the amphibian tree of life. Global Ecology and Biogeography 00:1–12.
Johnston, J. S., A. Bernardini, and C. E. Hjelmen. 2019. Genome size estimation and quantitative cytogenetics in insects. Methods in Molecular Biology 1858:15–26.
Khabbazian, M., R. Kriebel, K. Rohe, and C. Ané. 2016. Fast and accurate detection of evolutionary shifts in Ornstein–Uhlenbeck models. Methods in Ecology and Evolution 7:811–824.
Kidwell, M. G. 2002. Transposable elements and the evolution of genome size in eukaryotes. Genetica 115:49–63.
Kosch, T. A., A. J. Crawford, R. L. Mueller, K. C. W. Valero, A. Rodríguez, L. A. O'Connell, N. D. Young, et al. 2023. Comparative analysis of amphibian genomes: an emerging resource for basic and applied research. bioRxiv.
Kozłowski, J., M. Konarzewski, and A. T. Gawelczyk. 2003. Cell size as a link between noncoding DNA and metabolic rate scaling. Proceedings of the National Academy of Sciences of the United States of America 100:14080–14085.
Lamichhaney, S., R. Catullo, J. S. Keogh, S. Clulow, S. V. Edwards, and T. Ezaz. 2021. A bird-like genome from a frog: Mechanisms of genome size reduction in the ornate burrowing frog, *Platyplectrum ornatum*. Proceedings of the National Academy of Sciences 118:e2011649118.
Lanfear, R., P. B. Frandsen, A. M. Wright, T. Senfeld, and B. Calcott. 2016. PartitionFinder 2: New methods for selecting partitioned models of evolution for molecular and morphological phylogenetic analyses. Molecular Biology and Evolution msw260.
Levy, D. L., and R. Heald. 2016. Biological scaling problems and solutions in amphibians. Cold Spring Harbor Perspectives in Biology 8:a019166.
Licht, L. E., and L. A. Lowcock. 1991. Genome size and metabolic rate in salamanders. Comparative Biochemistry and Physiology Part B: Comparative Biochemistry 100:83–

92.
Liedtke, H. C., D. J. Gower, M. Wilkinson, and I. Gomez-Mestre. 2018. Macroevolutionary shift in the size of amphibian genomes and the role of life history and climate. Nature Ecology & Evolution 2:1792–1799.
Liedtke, H. C., J. J. Wiens, and I. Gomez-Mestre. 2022. The evolution of reproductive modes and life cycles in amphibians. Nature Communications 13:7039.
Lim, R. S. M., and T. Kai. 2015. A piece of the pi(e): The diverse roles of animal piRNAs and their PIWI partners. Seminars in Cell & Developmental Biology, Coding and non-coding RNAs & Mammalian development 47–48:17–31.
Lynch, M., and J. S. Conery. 2003. The origins of genome complexity. Science 302:1401–1404.
Lynch, M., B. Koskella, and S. Schaack. 2006. Mutation Pressure and the Evolution of Organelle Genomic Architecture. Science 311:1727–1730.
MacCulloch, R. D., D. E. Upton, and R. W. Murphy. 1996. Trends in nuclear DNA content among amphibians and reptiles. Comparative Biochemistry and Physiology Part B: Biochemistry and Molecular Biology 113:601–605.
Márquez, R., T. P. Linderoth, D. Mejía-Vargas, R. Nielsen, A. Amézquita, and M. R. Kronforst. 2020. Divergence, gene flow, and the origin of leapfrog geographic distributions: The history of colour pattern variation in *Phyllobates* poison-dart frogs. Molecular Ecology 29:3702–3719.
Mueller, R. L. 2015. Genome Biology and the Evolution of Cell-Size Diversity. Cold Spring Harbor Perspectives in Biology 7:a019125.
———. 2017. piRNAs and evolutionary trajectories in genome size and content. Journal of Molecular Evolution 85:169–171.
Mueller, R. L., T. Ryan Gregory, S. M. Gregory, A. Hsieh, and J. L. Boore. 2008. Genome size, cell size, and the evolution of enucleated erythrocytes in attenuate salamanders. Zoology 111:218–230.
Mulcahy, D. G., R. Ibáñez, C. A. Jaramillo, A. J. Crawford, J. M. Ray, S. W. Gotte, J. F. Jacobs, et al. 2022. DNA barcoding of the National Museum of Natural History reptile tissue holdings raises concerns about the use of natural history collections and the responsibilities of scientists in the molecular age. PLOS ONE 17:e0264930.
Myers, C. W., J. W. Daly, and B. Malkin. 1978. A dangerously toxic new frog (*Phyllobates*) used by Emberá Indians of western Colombia, with discussion of blowgun fabrication and dart poisoning. Bulletin of the American Museum of Natural History 161:307–366.
Oeldorf, E., M. Nishiokac, and K. Bachmann. 1978. Nuclear DNA amounts and developmental rate in holarctic anura. Journal of Zoological Systematics and Evolutionary Research 16:216–224.
Paradis, E., and K. Schliep. 2019. ape 5.0: An environment for modern phylogenetics and evolutionary analyses in R. Bioinformatics 35:526–528.
Pennell, M. W., J. M. Eastman, G. J. Slater, J. W. Brown, J. C. Uyeda, R. G. FitzJohn, M. E. Alfaro, et al. 2014. geiger v2.0: An expanded suite of methods for fitting macroevolutionary models to phylogenetic trees. Bioinformatics 30:2216–2218.
Piacentini, L., L. Fanti, V. Specchia, M. P. Bozzetti, M. Berloco, G. Palumbo, and S. Pimpinelli. 2014. Transposons, environmental changes, and heritable induced phenotypic variability. Chromosoma 123:345–354.
Pröhl, H. 2005. Territorial behavior in dendrobatid frogs. Journal of Herpetology 39:354–365.
Rabosky, D. L. 2014. Automatic Detection of Key Innovations, Rate Shifts, and Diversity-

Dependence on Phylogenetic Trees. PLOS ONE 9:e89543.
Rabosky, D. L., M. Grundler, C. Anderson, P. Title, J. J. Shi, J. W. Brown, H. Huang, et al. 2014. BAMMtools: An R package for the analysis of evolutionary dynamics on phylogenetic trees. Methods in Ecology and Evolution 5:701–707.
Rambaut, A., A. J. Drummond, D. Xie, G. Baele, and M. A. Suchard. 2018. Posterior summarization in Bayesian phylogenetics using Tracer 1.7. Systematic Biology 67:901–904.
Revell, L. J. 2012. phytools: An R package for phylogenetic comparative biology (and other things). Methods in Ecology and Evolution 3:217–223.
Reynolds, R. P., and R. D. MacCulloch. 2012. Preliminary checklist of amphibians and reptiles from Baramita, Guyana. Check List 8:211.
Rogers, R. L., L. Zhou, C. Chu, R. Márquez, A. Corl, T. Linderoth, L. Freeborn, et al. 2018. Genomic takeover by transposable elements in the Strawberry Poison Frog. Molecular Biology and Evolution 35:2913–2927.
Roth, G., K. C. Nishikawa, D. B. Wake, U. Dicke, and T. Matsushima. 1990. Mechanics and neuromorphology of feeding in amphibians. Netherlands Journal of Zoology 40: 115-135.
Santos, J. C. 2012. Fast molecular evolution associated with high active metabolic rates in poison frogs. Molecular Biology and Evolution 29:2001–2018.
Santos, J. C., M. Baquero, C. Barrio-Amorós, L. A. Coloma, L. K. Erdtmann, A. P. Lima, and D. C. Cannatella. 2014. Aposematism increases acoustic diversification and speciation in poison frogs. Proceedings of the Royal Society B: Biological Sciences 281:20141761.
Santos, J. C., and D. C. Cannatella. 2011. Phenotypic integration emerges from aposematism and scale in poison frogs. Proceedings of the National Academy of Sciences 108:6175–6180.
Santos, J. C., L. A. Coloma, and D. C. Cannatella. 2003. Multiple, recurring origins of aposematism and diet specialization in poison frogs. Proceedings of the National Academy of Sciences 100:12792–12797.
Santos, J. C., L. A. Coloma, K. Summers, J. P. Caldwell, R. Ree, and D. C. Cannatella. 2009. Amazonian amphibian diversity Is primarily derived from late Miocene Andean lineages. PLoS Biology 7:e1000056.
Santos, J. C., R. D. Tarvin, and L. A. O'Connell. 2016. A Review of Chemical Defense in Poison Frogs (Dendrobatidae): Ecology, Pharmacokinetics, and Autoresistance. Chemical Signals in Vertebrates 11. Springer, New York, NY.
Saporito, R. A., M. Isola, V. C. Maccachero, K. Condon, and M. A. Donnelly. 2010. Ontogenetic scaling of poison glands in a dendrobatid poison frog. Journal of Zoology 282:238–245.
Shine, R., and A. E. Greer. 1991. Why are clutch sizes more variable in some species than in others? Evolution 45:1696–1706.
Sidlauskas, B. 2008. Continuous and arrested morphological diversification in sister clades of Characiform fishes: A phylomorphospace approach. Evolution 62:3135–3156.
Silverstone, P. A. 1975. A revision of the poison-arrow frogs of the genus *Dendrobates* Wagler. Natural History Museum of Los Angeles County, Science Bulletin 21.
Silverstone, P. A. 1976. A revision of the poison-arrow frogs of the genus *Phyllobates* Bibron in Sagra (Family Dendrobatidae). Natural History Museum of Los Angeles County 27:1–53.
Smith, D. R. 2016. The mutational hazard hypothesis of organelle genome evolution: 10 years on. Molecular Ecology 25:3769–3775.
Specchia, V., and M. P. Bozzetti. 2021. The role of HSP90 in preserving the integrity of genomes against transposons is evolutionarily conserved. Cells 10:1096.

Stuckert, A. M. M., M. Chouteau, M. McClure, T. M. LaPolice, T. Linderoth, R. Nielsen, K. Summers, et al. 2021. The genomics of mimicry: Gene expression throughout development provides insights into convergent and divergent phenotypes in a Müllerian mimicry system. Molecular Ecology 30:4039–4061.

Summers, K., R. Symula, M. Clough, and T. Cronin. 1999. Visual mate choice in poison frogs. Proceedings of the Royal Society B: Biological Sciences 266:2141–2145.

Sun, C., D. B. Shepard, R. A. Chong, J. López Arriaza, K. Hall, T. A. Castoe, C. Feschotte, et al. 2012. LTR retrotransposons contribute to genomic gigantism in plethodontid salamanders. Genome Biology and Evolution 4:168–183.

Szczęsny, B., and R. J. Godunko. 2007. Caddis flies (Insecta: Trichoptera) in the collection of the State Museum of Natural History, National Academy of Sciences of Ukraine in Lviv. Acta Zoologica Cracoviensia - Series B: Invertebrata 50:27–43.

Taigen, T. L., and F. H. Pough. 1983. Prey preference, foraging behavior, and metabolic characteristics of frogs. The American Naturalist 122:509–520.

Tarvin, R. D., E. A. Powell, J. C. Santos, S. R. Ron, and D. C. Cannatella. 2017. The birth of aposematism: High phenotypic divergence and low genetic diversity in a young clade of poison frogs. Molecular Phylogenetics and Evolution 109:283–295.

Toft, C. A. 1995. Evolution of diet specialization in poison-dart frogs (Dendrobatidae). Herpetologica 51:202–216.

Tung Ho, L. si, and C. Ané. 2014. A linear-time algorithm for gaussian and non-gaussian trait evolution models. Systematic Biology 63:397–408.

Uyeda, J. C., M. W. Pennell, E. T. Miller, R. Maia, and C. R. McClain. 2017. The evolution of energetic scaling across the vertebrate tree of life. The American Naturalist 190:185–199.

Vacher, J.-P., P. J. R. Kok, M. T. Rodrigues, J. D. Lima, A. Lorenzini, Q. Martinez, M. Fallet, et al. 2017. Cryptic diversity in Amazonian frogs: Integrative taxonomy of the genus *Anomaloglossus* (Amphibia: Anura: Aromobatidae) reveals a unique case of diversification within the Guiana Shield. Molecular Phylogenetics and Evolution 112:158–173.

Vences, M., J. Kosuch, R. Boistel, C. F. B. Haddad, E. La Marca, S. Lötters, and M. Veith. 2003. Convergent evolution of aposematic coloration in Neotropical poison frogs: A molecular phylogenetic perspective. Organisms Diversity & Evolution 3:215–226.

Vinogradov, A. E. 1995. Nucleotypic effect in homeotherms: Body-mass-corrected basal metabolic rate of mammals is related to genome size. Evolution 49:1249–1259.

Werner, E. E. 1986. Amphibian metamorphosis: Growth rate, predation risk, and the optimal size at transformation. The American Naturalist 128:319–341.

Whitney, K. D., and T. Garland Jr. 2010. Did genetic drift drive increases in genome complexity? PLOS Genetics 6:e1001080.

Womack, M. C., M. J. Metz, and K. L. Hoke. 2019. Larger genomes linked to slower development and loss of late-developing traits. The American Naturalist 194:854–864.

Yang, Y., M. R. Servedio, and C. L. Richards-Zawacki. 2019. Imprinting sets the stage for speciation. Nature 574:99–102.